Nitric oxide inhibition of Drp1-mediated mitochondrial fission is critical for myogenic differentiation

Silvia Brunelli, Clara de Palma, Sestina Falcone, Serena Pisoni, Sara Cipolat, Chris Panzeri, Addolorata Pisconti, Raffaele Allevi, Maria Teresa Bassi, Giulio Cossu, et al.

Nitric oxide inhibition of Drp1-mediated mitochondrial fission is critical for myogenic differentiation

Clara De Palma[1*], Sestina Falcone[1*], Serena Pisoni[2], Sara Cipolat[3], Chris Panzeri[2], Sarah Pambianco[4], Addolorata Pisconti[1], Raffaele Allevi[4], Maria Teresa Bassi[2], Giulio Cossu[5.6], Tullio Pozzan[7], Salvador Moncada[8], Luca Scorrano[9], Silvia Brunelli[6,10§], and Emilio Clementi[1,2§].

[1]Unit of Clinical Pharmacology, Dept. of Preclinical Sciences, University Hospital "Luigi Sacco", Università di Milano, 20157 Milan, Italy; [2]E. Medea Scientific Institute, 23842 Bosisio Parini, Lecco, Italy; [3] Dulbecco-Telethon Institute, Venetian Institute of Molecular Medicine 35129 Padova, Italy; [4]Dept. of Clinical Sciences, University Hospital "Luigi Sacco", Università di Milano, 20157 Milan, Italy; [5]Dept. of Biology, Università di Milano, 20130 Milano, Italy; [6]San Raffaele Scientific Institute, 20132 Milano, Italy; [7]Venetian Institute of Molecular Medicine and Consiglio Nazionale delle Ricerche Institute of Neuroscience, Dept. of Biomedical Sciences, University of Padova, 35129 Padova, Italy; [8]The Wolfson Institute for Biomedical Research, University College London, London WC1E 6BT, UK; [9]Dept. of Cell Physiology and Metabolism, University of Geneva, 1211 Geneva, Switzerland; [10]Dept. of Experimental Medicine, University of Milano-Bicocca, 20052 Monza, Italy

*These authors contributed equally to the work

Running Title: NO controls mitochondrial fission and myogenesis

Key words: Nitric oxide, mitochondrial fission, Drp1, myogenesis

§ Corresponding authors:

Emilio Clementi, Dept Preclinical Sciences LITA-Vialba, University of Milano, via GB Grassi 74, 20157 Milano, Italy; Tel + 3902 5031 9686; Fax: +3902 50319646; E mail: emilio.clementi@unimi.it

Silvia Brunelli, San Raffaele Scientific Institute, Via Olgettina 60, 20132 Milano, Italy; Tel: +3902 2643 5066; Fax + 3902 2643 4813; E mail: brunelli.silvia@hsr.it

ABSTRACT

During myogenic differentiation the short mitochondria of myoblasts change into the extensively elongated network observed in myotubes. The functional relevance and the molecular mechanisms driving the formation of this mitochondrial network are unknown. We now show that mitochondrial elongation is required for myogenesis to occur and that this event depends on the cellular generation of nitric oxide (NO). Inhibition of NO synthesis in myogenic precursor cells leads to inhibition of mitochondrial elongation and of myogenic differentiation. This is due to the enhanced activity, translocation and docking to mitochondria of the pro-fission GTPase dynamin-related protein1 (Drp1), leading also to a latent mitochondrial dysfunction that increased sensitivity to apoptotic stimuli. These effects of inhibition of NO were not observed in myogenic precursor cells containing a dominant-negative form of Drp1. Both the NO-dependent repression of Drp1 action and the maintenance of mitochondrial integrity and function were mediated via the soluble guanylate cyclase. These data uncover a novel level of regulation of differentiation linking mitochondrial morphology and function to myogenic differentiation.

INTRODUCTION

Mitochondria are highly dynamic organelles that continuously and reversibly rearrange their structure through the tightly-regulated processes of fission and fusion of their inner and outer membranes [1, 2]. Mitochondrial fission is regulated by the GTPase dynamin-related protein 1 (Drp1) that cycles from the cytosol to mitochondria, where it binds to Fis1, an integral outer membrane protein, while fusion requires the activity of three large GTPase proteins, mitofusins 1 and 2 and optic atrophy 1 (Opa1) [3]. Mitochondrial dynamics participate in the cell response to fluctuations in oxygen and nutrient availability [4, 5] and contribute to regulation of the development and activity of a number of tissues and organs [6-8].

Despite the recognized role played by mitochondria in overall skeletal muscle function, including its repair after damage [9-11], the role of mitochondrial fission and fusion in skeletal muscle bioenergetics and development has not been investigated. Interestingly, during myogenic differentiation the short mitochondria of myoblasts change into the extensive elongated network observed in myotubes [12] suggesting that they may play a role in myogenesis.

We report here that inhibition of mitochondrial fission, with the consequent formation of a mitochondrial network, is required for myogenic differentiation, and that this is dependent on inhibition of Drp1 function. Furthermore, we report that endogenous nitric oxide (NO) generated by the muscle specific neuronal NO synthase (NOS) inhibits Drp1-dependent mitochondrial fission, and by this inhibition allows the process of myogenesis to occur. The action of NO was reversible (with a fast onset and offset), physiological, as it was mediated by cyclic GMP (cGMP), and was accompanied by profound changes in mitochondrial bioenergetics that play a role in myogenesis. Thus NO, by suppressing the activity of Drp1, allows the formation of

the mitochondrial network and the changes in cell bioenergetics needed for myogenesis to occur.

RESULTS

NO regulates myogenesis and mitochondrial elongation in differentiating myogenic precursor cells via cGMP

We examined the effects of endogenous generation of NO on myogenic differentiation and on changes in mitochondrial morphology. Myogenic precursor cells, freshly isolated from muscles of newborn mice, were transiently transfected with a red fluorescent protein targeted to mitochondria (mitoDsRed) and induced to differentiate [13]. Differentiating primary myogenic precursor cells (Fig. 1a) expressed progressively the differentiation markers Mef 2A, Myo D, myogenin and sarcomeric myosin (MyHC) (Fig. 1b and Supplementary Information, Fig. S1b). In parallel morphological studies, mitochondria that were round in shape in proliferating cells were found to become progressively elongated, forming an extensive branched network at 12 h of differentiation (Fig. 1a, and Supplementary Information: Fig. S1a for quantification of mitochondrial elongation and Fig. S2 for the 3D reconstructions). These changes in mitochondrial morphology were accompanied by changes in the expression of proteins regulating mitochondrial fission and fusion, namely Drp1, mitofusins and Opa1 (Fig. 1c and Supplementary Information, Fig. S1b). The increased expression of these proteins was not due to mitochondrial biogenesis since the expression of other mitochondrial proteins such as cytochrome *c* and cytochrome *c* oxidase did not change, neither did we detect an increase in mtDNA (Fig 1c and not shown). nNOS protein expression in differentiating cells was unchanged whereas NOS activity was increased, indicating that myogenic differentiation triggers NOS activation (Fig. 1d). The increased NOS activity was accompanied by increased generation of cGMP, a physiological messenger generated by NO through activation of guanylate cyclase (Fig. 1e) [14]. Both NOS activity and cGMP generation were

inhibited by the NOS inhibitor N$^{\omega}$-nitro-L-arginine methylester (L-NAME) (Fig.1, d and e). We examined the role of endogenous NO and cGMP generation on myogenic differentiation and mitochondrial morphology. L-NAME and the guanylate cyclase inhibitor H-(1,2,4)-oxadiazolo[4,3-]quinoxalin-1-one (ODQ) inhibited both the expression of myogenic markers (Fig. 1b) and the elongation of mitochondria (Fig. 1a and Supplementary Information, Fig S1). Inhibition of NO or cGMP generation did not modify the expression of the mitochondria-shaping proteins or of mtDNA (Fig. 1c and not shown). The neuronal NOS splice variant μ is particularly important in muscle physiology [15]. Silencing of the enzyme using a specific siRNA, inhibited expression of myogenic differentiation markers and elongation of mitochondria (Supplementary Information, Fig. S3), indicating that NO generation and the consequent elevation of cGMP are required for both mitochondrial elongation and myogenesis.

Changes in mitochondrial morphology may be the consequence of toxic cellular effects. In differentiating myoblasts neither L-NAME nor ODQ induced significant changes in the basal rate of apoptosis, assessed up to 72 h of differentiation by measuring phosphatidylserine exposure to the plasma membrane in 7-amino actinomycin D-excluding cells (Fig 2a) and the number of trypan-blue excluding (viable) cells (Fig. 2b). Consistently, we did not observe activation of caspases 3 and 9 (Fig 2c). Likewise, neither ODQ nor L-NAME induced spontaneous apoptosis in proliferating, undifferentiated myoblasts (not shown). These results rule out a toxic action by L-NAME and ODQ.

NO/cGMP stimulate myogenesis through inhibition of mitochondrial fission

Myogenic precursor cells were co-transfected with vectors coding for mitoDsRed and cytosolic YFP (pEN1YFP). After induction of differentiation for 6 h we investigated by real time confocal microscopy and transmission electron microscopy the effects of L-NAME and ODQ on mitochondrial morphology. Differentiation for this period resulted in the majority of mitochondria being in the elongated form (Fig 3b and 3c). However, both L-NAME and ODQ induced mitochondrial fragmentation within minutes after their addition, which persisted throughout the time of analysis (40 min) and was confirmed at the ultrastructural level (Fig. 3a and Supplementary Information, Fig S4 for electron microscopy images and Fig. S5 for the films). The NO donor (Z)-1-[2-(2-aminoethyl)-*N*-(2-ammonioethyl) amino]diazen-1-ium-1,2 diolate (DETA-NO) and the membrane-permeable cGMP mimic 8 Br-cGMP reversed the effects of L-NAME and ODQ, respectively, indicating the cGMP-dependency of the action of NO (Fig. 3, b and c). These results indicate that changes in mitochondrial morphology are due to actions of NO/cGMP.

Mitochondrial dynamics depend on the processes of fission and fusion [1, 2]. We investigated whether NO/cGMP regulates fission, fusion or both processes. To examine mitochondrial fusion, we performed a polyethylene glycol fusion assay on myoblasts differentiated for 6 h. Neither L-NAME nor ODQ changed the rate of mitochondrial fusion, monitored by measuring the appearance of double mtRFP/mtGFP-positive mitochondria in the heteropolykaryons in the presence of cycloheximide for a further 6 h after polyethylene glycol addition (Fig. 4, a and b). However, a dominant negative (K38A) mutant of Drp1 [16] prevented the effects of L-NAME and ODQ on mitochondrial morphology (Fig. 4c). This mutant also prevented the slowing of myogenic differentiation induced by L-NAME and ODQ and enhanced

the myogenic process, most likely by inhibiting basal Drp1 function (Fig. 4d and Supplementary Information, Fig. S6). These results demonstrate that mitochondrial elongation by NO is due to reduced fission and that this modulation regulates myogenesis.

NO/cGMP control Drp1 localization and activity

To investigate how NO regulates Drp1 function via cGMP we monitored the activity and subcellular localization of Drp1 in differentiating myoblasts. Subcellular fractionation and immunoblotting for Drp1 showed that mitochondrial Drp1 localization was significantly increased by L-NAME and ODQ (Fig. 5a). In addition, ODQ and L-NAME increased the interaction between Drp1 and its mitochondrial receptor Fis1, as demonstrated by co-immunoprecipitation (Fig. 5b and not shown). Finally, L-NAME and ODQ increased the binding of Drp1 to GTP, an assay that measures GTPase activity in intact cells, as shown by pull-down experiments using GTP-conjugated beads (Fig. 5c). DETA-NO or 8Br-cGMP reversed all the effects of L-NAME and ODQ, respectively. Of note, we did not detect any significant changes in mitochondrial and cytosolic calcium concentrations upon NOS or guanylate cyclase inhibition, thereby ruling out calcium overload as a trigger for fission in these conditions (not shown). Drp 1 is known to be regulated via protein kinase A and C through phosphorylation. We investigated whether NO/cGMP acting via G kinase induced phosphorylation of Drp1. As shown in Fig. 6a myogenic differentiation was accompanied by phosphorylation of Drp1 which was prevented by both L-NAME and ODQ. In addition, DETA-NO and 8 Br-cGMP induced phosphorylation of the protein in a way that was prevented by the G kinase inhibitor KT5823 and enhanced by BAY41-2272, that activates guanylate cyclase independently of NO (Fig. 6b). These

experiments indicate that NO/cGMP phosphorylates Drp1 via G kinase and inhibits its function during myogenic differentiation.

NO/cGMP maintain mitochondrial membrane potential in differentiating myoblasts

We investigated whether changes in mitochondrial morphology and dynamics affected the bioenergetics of differentiating myoblasts, using the F_1F_0 ATP synthetase inhibitor oligomycin; this is used as a sensitive test of latent mitochondrial dysfunction in intact cells [17]. In proliferating myogenic precursor cells and in control differentiating myoblasts (6 h) oligomycin increased the mitochondrial membrane potential, as indicated by an increase in the mitochondrial fluorescence of the potentiometric dye tetramethyl rhodamine methyl ester (TMRM) followed by real-time imaging (Fig. 7a); this is as expected for healthy mitochondria [17]. By contrast, in L-NAME or ODQ-treated differentiating myoblasts the addition of oligomycin led to progressive mitochondrial depolarization, which was fully normalized by Drp1 K38A (Fig. 7a and not shown), establishing a link between changes in mitochondrial dynamics and mitochondrial membrane potential. L-NAME and ODQ had no effects on the mitochondrial membrane potential in proliferating cells (not shown). These findings suggest that if NO or cGMP is depleted during myogenesis the fragmented mitochondria that result will display a latent mitochondrial dysfunction.

NO/cGMP regulate mitochondrial respiration and ATP generation in differentiating myoblasts

We next investigated the effects that the latent dysfunction observed in mitochondria had on the bioenergetic parameters of differentiating myoblasts, in which NO or

cGMP generation was inhibited. Total OXPHOS-ATP, measured in the presence of the glycolysis inhibitors fluoride and iodoacetate, was significantly reduced in ODQ- or L-NAME-treated differentiating cells compared to that in untreated controls. The effects of L-NAME or ODQ were abolished by Drp1 K38A (Fig. 7b and not shown). The amount of ATP generated normally by glycolysis was low in each treatment group, with no significant changes induced by ODQ/L-NAME or Drp1 K38A (Fig. 7c).

We analysed cell respiration (time 6 h) measuring total, oligomycin-resistant (proton leak) and maximal (uncoupled) oxygen consumption in proliferating and differentiating myogenic cells. ODQ and L-NAME did not significantly alter total, oligomycin-resistant or maximal oxygen consumption in proliferating cells (not shown), whereas they reduced all respiratory parameters in differentiating cells (Fig. 7d). Neither L-NAME nor ODQ had any effect on the residual, mitochondrial-independent oxygen consumption (ROC in Fig 7d). To further assess the functional relevance of the changes induced by L-NAME and ODQ on respiration we measured the ratios of oligomycin-resistant to maximal oxygen consumption and coupled respiration (total minus the oligomycin resistant oxygen consumption) to maximal. These rates give an estimate of whether changes in total respiration can ultimately affect the ability of the mitochondria to utilize the proton-motive force to synthesize ATP. In ODQ- or L-NAME- treated cells, the ratio of oligomycin resistant to the maximal respiration was reduced, while the ratio of coupled respiration to maximal was increased (Fig. 7e and not shown). These data indicate that cells try to compensate for the reduced respiratory capacity induced by impairment of NO or cGMP signalling with enhanced coupling of electron transport with oxidative phosphorylation. All changes induced by L-NAME or ODQ were prevented by Drp1

K38A, indicating that impairment of respiratory function induced by L-NAME or ODQ in differentiating myogenic precursor cells is a consequence of changes in mitochondrial dynamics. The use of selective inhibitors of the electron transport chain demonstrated that L-NAME and ODQ decrease mitochondrially generated ATP regardless of which mitochondrial complex was stimulated (Fig. 7f and not shown), suggesting that cytochrome *c* oxidase, the terminal component of the respiratory chain, is the likely target. As with the other parameters investigated, mitochondrial complex activities were restored by Drp1 K38A.

NO/cGMP and mitochondrial dynamics: a quality control check for myogenesis

To investigate the functional role of the induction of fission and the resulting impaired mitochondrial function, we examined cell sensitivity to oxidative stress. In differentiating myoblasts, apoptosis induced by H_2O_2 was significantly increased in cells in which NO/cGMP signalling was blocked by L-NAME or ODQ (Fig 8). Such increased sensitivity was Drp1-dependent, as demonstrated by its absence in the K38A mutant. No differences in H_2O_2-induced apoptosis were observed in proliferating cells exposed to ODQ or L-NAME (not shown). These results indicate that in differentiating myoblasts impairment of NO/cGMP signalling and the ensuing changes in mitochondrial function lead to an increased sensitivity to apoptogenic stimuli.

DISCUSSION

In this study we demonstrate that inhibition of NOS activity prevents elongation of mitochondria and myogenesis, indicating that NO plays a determinant role in these processes, by controlling the function and activity of the mitochondrial fission protein Drp1. Indeed the expression of the dominant-negative form of Drp1 K38A reversed the effects due to removal of NO on both control of mitochondrial dynamics and myogenesis. These effects were specific to differentiating myoblasts since NO had no effect on mitochondrial shape or activity in proliferating myogenic precursors cells. The effects of NO were dependent on activation of guanylate cyclase and the generation of cGMP, which is activated by nanomolar concentrations of NO [18]. This indicates that the process described takes place under physiological conditions.

NO/cGMP acted selectively on mitochondrial fission, directly controlling Drp1 GTPase activity, translocation to mitochondria and interaction with Fis1. Drp1 activity is known to be tightly regulated through phosphorylation by both the cyclin-dependent kinase 1 and the cAMP-dependent protein kinase, and by dephosphorylation mediated by calcineurin [19, 20]. Our results show that NO phosphorylates Drp1 via G kinase. This kinase-dependent mechanism of control of Drp1 suggests the need for additional tight levels of regulation of the enzyme, and stresses the importance of this mechanism and the biological relevance of its control by NO. Furthermore, the fact that NO regulates the activity and not the expression of Drp1 points towards a dynamic role of fission control by NO that may be relevant to fine-tuning the process of myogenesis.

In neurons high, cytotoxic concentrations of NO have been reported to promote fission and apoptosis and may contribute to the pathogenesis of Alzheimer's disease [21, 22]. This effect is mediated by S-nitrosylation of Drp1 [23] , *i.e.* a mechanism different

from the cGMP/G kinase-dependent phosphorylation we show here and that activates rather than inhibits the enzyme. These findings, although apparently contradictory to the results reported here, are in keeping with the concept that NO is a double-edged messenger that, depending on its concentration and mechanism of action, can have opposing effects on a particular mechanism or target [24, 25]. Likewise, the role of Drp1 and fission differ depending on cell type, due to differences in cell management of mitochondrial morphology and function. Drp1-null embryos fail to undergo developmentally regulated apoptosis during neural tube formation in vivo while embryonic fibroblasts have normal apoptotic responses,[26].

The specific role of NO in regulating myogenesis physiologically via a mitochondrially-linked mechanism raises the question of the biological significance of such control. A possible answer lies in the NO-dependent bioenergetic changes taking places in mitochondria of differentiating myoblasts and in their pathophysiological consequences that we describe here.

Although the mitochondrial membrane potential was maintained in cells in which fission was taking place as a result of the lack of NO/cGMP, its collapse following treatment with the F_1F_0 ATP synthetase inhibitor oligomycin and the low rate of ATP generation observed in these conditions revealed that mitochondrial respiration is impaired. Such reduced activity was a consequence and not a cause of mitochondrial fission, since it was reversed by Drp1 K38A. The functional consequence of such a metabolic defect was evident when apoptosis was induced, so that cells in which fission was taking place were more sensitive to an apoptogenic stimulus. It is possible that mitochondria and NO act as a quality control check of myogenesis. Indeed activation of NOSs depends critically on the correct architecture of cells and on intracellular signalling pathways that may be disrupted in damaged cells [18, 27].

The metabolic changes subsequent to the NO/cGMP-dependent changes in mitochondrial dynamics appear to follow changes in cytochrome *c* oxidase activity. A recent study highlighted how this enzyme is regulated by cAMP, with important metabolic consequences [22], in a manner analogous to the Drp-1-mediated, cGMP-dependent mechanism described here. These observations reveal new and significant mechanisms of regulation of cytochrome *c* oxidase, with biological consequences that add to the complexity and recognized importance of this enzyme for cell pathophysiology [28-30].

Previous studies have shown that expression of NOSs is developmentally-regulated and that NO acts at various levels in the process of myogenesis, by increasing secretion of follistatin and follistatin-1-like proteins [31-33] and cooperating with insulin-like growth factor II [34]. In addition, it favours activation, proliferation and engraftment of myogenic stem cells [13, 35, 36]. We now show that NO controls early events in myogenic differentiation. It appears therefore that NO presides over several critical steps of muscle differentiation that are important in repair, and may explain why NO-based therapies appear to work effectively in reducing muscle damage in muscular dystrophy [31, 35].

The fact that the action of NO is mediated via inhibition of mitochondrial fission and changes in metabolic status of mitochondria is of great physiological importance in muscle. In particular, NO controls mitochondrial respiration through reversible inhibition of cytochrome *c* oxidase, acting as an acute sensor for changes in the oxygen concentration [37, 38]. In addition, it stimulates mitochondrial biogenesis [39, 40], a key event occurring in muscle hypertrophy and muscle repair that also contributes to definition of the slow twitch-oxidative *vs.* fast twitch-glycolytic nature of muscle fibres [9, 11, 15, 41]. We now describe a third action aimed at regulating mitochondrial

dynamics and the resulting changes in bioenergetics. Oxygen sensing and mitochondrial fission are regulated acutely by NO, whereas mitochondrial biogenesis requires sustained changes in NO concentration [38, 39]. Understanding whether these actions of NO are independent from each other or are causally linked, in particular if the acute NO-regulated effects on mitochondria influence mitochondrial biogenesis, may lead to a better understanding of the role of NO in modulating mitochondrial behaviour, giving new insights into the importance of energy metabolism in the control of muscle development and regeneration. In view of the role of NO and mitochondrial dysfunction in muscle degenerative diseases [35, 42-44], these findings will be critical for designing novel therapeutic approaches to these pathological conditions.

MATERIALS AND METHODS

Cell culture and treatment

Myogenic precursor cells were prepared as previously described [45]. Briefly, muscle fragments were digested with 2% collagenase II and dispase (Sigma and Gibco-Invitrogen) for 10 min at 37°C with gentle agitation. Dispersed cells were then collected, pooled, centrifuged, resuspended in Iscove's modified Dulbecco's medium supplemented with 20% fetal bovine serum, 3% chick embryo extract [45], 100 U/ml penicillin, 100 μg/ml streptomycin and 50 μg/ml gentamycin, and plated onto matrigel-(BD Transduction Laboratories) coated dishes at a density of 10^4 cells×cm^2. Contamination by non-myogenic cell was reduced by pre-plating the cell suspensions onto plastic dishes where fibroblasts tend to adhere more rapidly. Differentiation was induced by changing the medium to Iscove's modified Dulbecco's medium supplemented with 2% horse serum.

Drug treatments were as follows: myogenic precursor cells were differentiated for 6 h and then treated with L-NAME (1 mM), ODQ (1 μM), DETA-NO (30 μM) and 8Br-cGMP (1 mM), alone or in combination, except for time-course differentiation experiments in which drugs were added immediately after changing to differentiation medium.

DNA constructs and cell transfections

Drp1 was purchased from OriGene technologies and subcloned in pcDNA4/myc-His (Invitrogen) using the following primers containing the sequences for 2 restriction sites: EcoRV (CGG ATA TCG TCA TGG AGG CGC TAA TTC CT) and XhoI (CCT CGA GGT CAC CAA AGA TGA GTC TCC). PCR conditions, using the Pfu high fidelity polymerase (Stratagene) were as follows: 95°C for 2 min, then 4 cycles

as follows: 95°C for 30 s, 50°C for 30 s, 72°C for 5 min and then 25 cycles as follows: 95°C for 30 s, 60°C for 30 s, 72°C for 5 min. The fragment of 2208 bp thus obtained was subcloned in pcDNA4/mycHys (Invitrogen) XhoI-EcoRV linearized vector, upstream of the Myc tags.

Generation of the Drp1 K38A was obtained through site-directed mutagenesis of pcDNA4-Myc-Drp1 using a QuikChange II Site-directed Mutagenesis Kit (Stratagene, La Jolla, CA, USA). The endogenous Drp1 stop codon was removed using the following primers: 5'GGA GAC TCA TCT TTG GTC CTC GAG TCT AGA GGG CCC G 3'(sense); 5'CGG GCC CTC TAG ACT CGA GGA CCA AAG ATG AGT CTC C 3' (antisense). The second mutagenesis step to obtain Drp1 K38A was performed with the following primers: 5' GGG AAC GCA GAG CAG CGG AGC GAG CTC AGT G 3' (sense); 5' CAC TGA GCT CGC TCC GCT GCT CTG CGT TCC C 3' (antisense). The constructs were sequence-verified with a Big Dye Terminator Sequencing Kit (version 3.1, Applied Biosystems), run on an Applied Biosystems ABI 3100 Avant Genetic Analyzer.

In order to obtain the construct pEYFP-N1-Drp1 and pEYFP-N1-Drp1K38A, the original OriGene construct was digested with Not1 and the Drp1 fragment was subcloned in Not1 linearized pEYFP-N1 (Invitrogen) downstream to YFP. Site-specific mutagenesis was performed first to remove a stop codon in the EYFP sequence using the following primers: 5' CTC GGC ATG GAC GAG CTG TAC AAG AGC AAG GCC GCG AAT TC 3' (sense); 5' GAA TTC GCG GCC TTG CTC TTG TAC AGC TCG TCC ATG CCG AG 3' (antisense). Drp1K38A was finally obtained with a second mutagenesis step as described above. The final constructs were verified by sequencing, as described above.

Cell transfections were performed with the FuGENE HD reagent (Roche) according to the manufacturer's instructions. Cells were used 24 hours after transfection in the various experimental settings described.

To silence nNOS we used the "ON-TARGETplus SMARTpool siRNA" system developed by Thermo Scientific Dharmacon laboratories (Lafayette, CO, USA) in which silencing is obtained by transfection of 40 nM of a pool of four different siRNAs. The nNOS-silencing siRNA used in the pool were CCA AAG CUG UCG AUC U; GAU CCA ACC CAA CGU CAU U; GCA GAG CGG CCU UAU CCA A; GAU GAA AGA CAC AGG AAU C. Transfections were carried out using the INTERFERIN polyplus transfection reagent from Euroclone.

Immunoblotting

Extracted proteins (50 μg) were separated by 4-12% SDS-PAGE (NuPAGE, Invitrogen) and transferred onto nitrocellulose membranes (Perkin Elmer) as described [46]. Membranes were probed using the following antibodies (Abs): anti-calnexin (1:5000, Genetex, Inc); anti-Mfn2 (1:200, Abnova); anti-Mfn1 (1:200, Abnova); anti Drp1 (1:1000, BD Transduction); anti-COXIV(oxidative phosphorylation Complex IV subunit IV; 1:400, Molecular Probes); anti-Myc (1:1000, Cell Signaling Celbio); anti-MyoD (1:500, DakoCytomation), anti–sarcomeric myosin MyHC (1:10, Developmental Studies Hybridoma Bank), anti myogenin (1:10, Developmental Studies Hybridoma Bank); anti Mef2A (1:500, Santa Cruz Biotechnology), anti GADPH (AbD Seretoc) and anti Opa1 (1:1000, BD Transduction).

Assay of NOS activity

The time course of NOS activity was assayed in intact cells by measuring the conversion of L-[^{3}H]-arginine into L-[^{3}H]-citrulline [46]. In brief, the reaction was performed in 145 mM NaCl, 5 mM KCl, 1 mM $MgSO_4$, 10 mM glucose, 1 mM $CaCl_2$, and 10 mM HEPES, pH 7.4. A mix of 10 μCi/ml L-[^{3}H]-arginine and 10 μM of cold arginine was added at various time points, and the reaction stopped after 5 min by washing with ice-cold PBS supplemented with 5 mM L-arginine and 4 mM EDTA. 0.5 ml of 100% cold ethanol was added to the dishes and left to evaporate before a final addition of 20 mM HEPES, pH 6.0. L-NAME–treated cells were run in parallel as a control of specificity. Separation of L-[^{3}H]-citrulline from L-[^{3}H]-arginine was performed by DOWEX 50X8-400 chromatography. L-[^{3}H]-citrulline formed was normalized to protein content, which was evaluated by the bicinchoninic acid procedure (BCA, Perbio Bezons).

Measurement of cGMP generation

At each time point, myogenic precursor cell cultures were incubated for 30 min at 37°C either in growth or in differentiation medium with 0.5 mM of the phosphodiesterase inhibitor 3-isobutyl-1-methylxanthine, supplemented with 1 mM L-NAME, or vehicle [46]. The reaction was terminated by rapid removal of medium and washing with ice-cold PBS. Cells were lysed by the addition of ice-cold trichloroacetic acid (final concentration: 6%). After ether extraction, cGMP levels were measured using a radioimmunoassay kit and normalized to protein content.

Confocal and time -lapse microscopy

For confocal *z*-axis stacks of mitochondrial network, coverslips were placed on the stage of an UltraVIEW ERS Spinning Disk Confocal microscope equipped with a stage incubator from OkoLab and an EM-CCD Hamamatsu C9100, allowing us to follow highly dynamic processes. Cells expressing mtDsRed [47] were excited using the 514-nm line of the HeNe laser with exposure times of 100 msec using a 63x immersion objective. Stacks of 20 images, separated by 1 μm along the *z*-axis, were acquired for steady-state and time-resolved 3D imaging. Total acquisition time for each stack was 1.1 sec for the 20 planes to minimize reconstruction artifacts caused by mitochondrial movement. Reconstruction of the stacks was performed with Volocity software.

For confocal imaging of fixed cells, 16-mm round coverslips were placed on the stage of a Leica TCS SP2 Laser Scanning Confocal with an electronically controlled and freely definable Acousto-Optical Beam Splitter. Images were acquired with 63x magnification oil immersion lenses at 1024 · 1024 pixel resolution. Cells were excited with the 543-nm line for mtDsRed, and emitted light was collected with 570 long-pass filters. Morphometric analyses were performed with imagetool 3.0 (University of Texas Health Science Center, San Antonio). Images of cells expressing mitoGFP or mitoDsRed [47] were thresholded by using the automatic threshold function. For each identified object, the major axis length and the roundness index were calculated. Cells were scored with elongated mitochondria when >50% of the objects in the image (i.e., mitochondria) displayed a major axis longer than 5 mm and a roundness index below 0.5 (maximum value is 1).

Serial images (z-stacks) of mitoDsRed-expressing myogenic cells were acquired with a Leica TCS SP2 Laser Scanning Confocal microscope and collected with a z-step of

0.5 μm. Image analysis and processing was performed with the public domain software MBF_ImageJ for Microscopy (http://www.macbiophotonics.ca/index.htm). Single channel surface-rendered images were processed with ImageJ running the VolumeJ plugin [48] as described[49].

Electron transmission microscopy

After the various treatments, myogenic precursor cell pellets were prepared for electron microscopy, as described [39]. In brief, thin sections were obtained with a MT-X ultramicrotome (RMC, Tucson, Arizona, USA), stained with lead citrate and examined with a transmission electron microscope (Philips CM10, Eindhoven, The Netherlands). A minimum of 50 cells from each treatment were assessed.

Apoptotic cell death analysis

For cell death experiments, cells were plated in 6-well dishes, exposed to the treatments indicated in the section "Cell culture and treatment" and treated in the presence or absence of 30 μM H_20_2 for 4 h at 37°C. Cell were detached and stained with tetramethyl rhodamine isothiocyanate-annexin V 1:20 and 7-amino actinomycin D 1:5 (7AAD; BD Bioscience) according to the instructions of the manufacturer of the kit and analyzed by flow cytometry in a FACStar Plus (Becton Dickinson) as described [13]. Cells staining positive for Annexin V and excluding 7AAD were considered to be apoptotic. Cell death was assessed also by the trypan blue exclusion assay of cell viability and by detecting activated caspase3 and caspase9 with specific Abs (Cell Signaling-New England Biolabs).

Polyethylene Glycol (PEG) Fusion Assay

Fusion experiments were carried out as described [47]. In brief, 5×10^5 mouse myogenic precursor cells were transfected either with mitoGFP or with mitoDsRed alone. After 24 h, the cells labeled with different fluorescent proteins were co-plated at a 1:1 ratio onto 13-mm round coverslips. Differentiation was induced for 6 h after which cells were treated with L-NAME or ODQ for 1 h; fusion was induced by a 60-sec treatment with a 50% (wt/vol) solution of PEG 1500 in PBS (Sigma), followed by extensive washes in DMEM supplemented with 10% foetal calf serum. To inhibit *de novo* synthesis of fluorescent proteins, 30 min before PEG treatment cells were incubated with the protein synthesis inhibitor cycloheximide (20 μg/ml, Sigma), which was subsequently kept in all solutions and tissue culture media until cells were fixed for 30 min with ice-cold 3.7% (vol/vol) formaldehyde in PBS. After two washes with PBS, the coverslips were mounted on slides with Anti-Fade Reagent (Molecular Probes). For imaging of polykaryons, fixed cells on 13-mm round coverslips were placed on the stage of a BioRad MRC 1024 Laser Scanning Confocal microscope. Cells were excited with the 488-nm laser line for yellow fluorescent protein and the 568-nm line for mitoDsRed, and emitted light was collected with 515/30 band-pass and 570 long-pass filters, respectively. The intensity of double-labelling in polykaryons was quantified in three different experiments using the "Colocalizer" plugins of ImageJ software.

Subcellular fractionation

Myogenic precursor cells were scraped in 400 μl of homogenization medium (0.3 M sucrose, 10 mM MES K^+, 1mM K_2EGTA, 1 mM Mg_2SO_4, protease inhibitors, pH 7.4) and homogenized with 25 strokes of a ball-bearing homogenizer on ice before

centrifugation at 1000x g for 10 min at 4°C. The resulting low-speed pellet containing nuclei and unbroken cells was discarded. The post nuclear supernatant (PNS) was further centrifuged at 10000x g for 30 min at 4°C and the resulting pellet contained both heavy and light mitochondrial fractions. The pellet was washed twice at 10000x g for 30 min at 4°C. The post mitochondrial supernatant was centrifuged at 55000x rpm for 2 h with TLA-100 to obtain a microsomal pellet and a cytosolic fraction. Equal amounts of mitochondria, microsomes and cytosolic fraction were separated on 12% polyacrylamide gel, blotted onto a nitrocellulose membrane (Perkin Elmer) and probed with anti-Drp1 anti- COX IV, anti GADPH Abs [50].

Detection of the interaction between Fis1 and Drp1 by co-immunoprecipitation

To test for a Drp1-Fis1 interaction in intact cells, in view of the reversible nature of such an interaction, myogenic precursor cells were subjected to chemical cross-linking. The cleavable, homo-bifunctional cross-linker dithiobis (succinimidylpropionate) (DSP; Pierce Chemical Co.) was diluted to a 1.0 mM final concentration in phosphate-buffered saline and added to cultured cells. After incubation for 1 h at room temperature, cross-linking was stopped by the addition of Tris HCl (pH 7.7) to a final concentration of 20 mM. Cells were lysed with lysis buffer containing 20 mM Tris HCl, 150 mM NaCl, 10 mM EGTA, 10% glycerol and 1% Triton X-100, pH 7.4, and the immunoprecipitation was performed with anti-Fis1 Abs and protein A-Sepharose (GE Healthcare) for 16 h at 4°C. Samples were washed three times in lysis buffer and boiled in sodium dodecyl sulfate sample buffer containing 5% 2-mercaptoethanol to cleave the cross-linking. Samples were run on 15% polyacrylamide gels and subjected to western blot analysis with anti-Drp1, anti-Fis1 Abs (Alexis Biochemicals). Specificity of the interaction between the two

proteins and of the binding to the beads was verified in a control immunoprecipitation experiment with an anti-Calnexin Ab (Genetex), followed by immunoblotting with anti Drp1 or Fis1 Abs.

Assay for GTPase activity

Cells were suspended in 400 µl homogenization buffer containing 0.22 M mannitol, 0.07 M sucrose, the protease inhibitor cocktail and 10 mM HEPES-KOH, pH 7.4, and homogenized with ten strokes using a syringe equipped with a 27-gauge needle. The post nuclear supernatant was recovered by centrifugation at 1500 rpm for 5 min and 300 µl were diluted in a reaction buffer (homogenization buffer containing 50 mM Tris-HCl, 150 mM NaCl, 1 mM $MgOAc_2$, 1 mM dithiothreitol, protease inhibitor cocktail and 1% digitonin, pH 7.5). The cleared lysate was incubated with 30 µl GTP-agarose beads (Sigma) at 30°C for 1 h. The beads were washed three times in the same buffer. The proteins were resolved by sodium dodecyl sulfate polyacrylamide gel electrophoresis and analyzed by immunoblotting using anti-Drp1 Abs [51].

Measurement of Ca^{2+} concentrations

Cells grown on 13 mm round glass coverslips at 50% confluence were co-transfected with cytosolic, or mitochondrial aequorin [52]. Aequorin reconstitution, measurement and calibration were performed in a Krebs Ringer HEPES buffer containing 1 mM Ca^{2+}, pH 7.4. All measurements were carried out in this buffer [52].

Measurement of mitochondrial membrane potential

Cells were seeded onto 24-mm-diameter round glass coverslips and mitochondrial membrane potential was measured based on the accumulation of TMRM (Molecular

Probes Invitrogen) as described [17]. Cells were rinsed once and then incubated in serum-free Hank's buffered salt solution, supplemented with 1.6 μM cyclosporine H to minimize variability in the extent of mitochondrial loading with potentiometric probes, and loaded with 10 nM TMRM for 30 min. One μg/ml of oligomycin was added during time lapse as indicated in the figures and, at the end of each experiment, mitochondria were fully depolarized by the addition of 4 μM of the protonophore carbonyl cyanide p-trifluoromethoxy phenylhydrazone (FCCP). Cellular fluorescence images were acquired using the epifluorescence-based IN Cell Analyzer 1000 microscope system (GE Healthcare) equipped with a high resolution CCD camera, fast laser-based confocal auto focus, and optical Z sectioning with Opti-Grid. Images were analyzed using the IN Cell Investigator Software for automated analysis of cellular images. Sequential digital images were acquired every 1 min, and the average fluorescence intensity of all relevant regions was recorded and stored for subsequent analysis [17].

Measurement of ATP formation

ATP concentration was determined using the Luciferin-Luciferase method [53]. Briefly, cells were resuspended in buffer A (150 mM KCl, 25 mM Tris-HCl, 2 mM EDTA, 0.1% BSA, 10 mM potassium phosphate and 0.1 mM MgCl, pH 7.4) and incubated for 1 min with 50 μg/ml of digitonin at room temperature with gentle agitation. They were then washed by adding 1 ml of bufferA and pelletted at 1000 g. Cell pellets were resuspended in 160 μl of buffer A and plated in 96 wells in triplicate. Samples were treated with 30 μl of mix containing 1 mM malate, 1 mM pyruvate, 0.1 mM ADP (Sigma), 10 μl buffer B (containing 0.8 mM luciferin and 20 mg/ml luciferase in 0.5 M Tris-Acetate pH 7.75) and either 1 μg/ml oligomycin or 100 μM iodoacetate or 4

mM fluoride to assess OXPHOS ATP and glycolytic ATP, respectively. ATP was measured using a GloMax luminometer (Promega).

Tests for respiratory chain defects were essentially performed as described [54]. In brief, digitonin-permeabilized cells were incubated at 37°C for 15 min in a buffer containing 0.25 M sucrose, 20 mM MOPS, 1 mM EDTA, 5 mM inorganic phosphate, 0.1% fatty acid-free BSA, and 1 mM ADP, pH 7.4, and supplemented with the following specific substrates and inhibitors of the respiratory chain complexes: 1 mM pyruvate and 5 mM malate, or 5 mM glutamate and 5mM malate (complex I); 1 μM rotenone and 10 mM succinate (complex II); 10 μg/ml antimycin A, 0.1 mM N,N,N'-N'-tetramethyl-p-phenylenediamine and 2 mM ascorbate (complex IV).

Analysis of phosphorylation of Drp1

Myogenic precursor cells were transfected with pcDNA3-Drp1-myc and its control empty vector. After 24 h, myogenic precursor cells were differentiated for 6 h, incubated in serum-free medium and labelled with 0.5 mCi/ml [^{32}P]orthophosphate (8500-9120 Ci/mmol; PerkinElmer Life Science) for 3.5 h in the presence of 100 μM 3-isobutyl-1-methylxanthine. To determine the role of NO directly, cells were incubated in serum-free medium containing 0.5 mCi/ml [^{32}P]orthophosphate for 3 h and treated with 30 μM DETA-NO, 1 μM KT5823, 1 mM 8Br cGMP, 1 μM ODQ and 2 μM BAY41-2272 for 1.5 h, in the presence of 100 μM 3-isobutyl-1-methylxanthine. Cells were lysed in a radioimmunoprecipitation buffer supplemented with a protease inhibitor mixture (Sigma-Aldrich) and a phosphatase inhibitor mixture (Sigma-Aldrich). Myc-Drp1 was immunoprecipitated using an anti-Myc monoclonal Ab (9E10) immobilized on agarose beads (Invitrogen). Immunoprecipitates were

resolved by SDS-PAGE and ^{32}P-labelled Drp1 was visualized by autoradiography using Amersham Hyperfilm ^{TM} MP (GE Healthcare).

High Resolution Respirometry

The respiration rate of myogenic precursor cells transfected with pEYFP-N1 Drp1 K38A or empty vector, differentiated for 6 h and treated with ODQ for 1 h, was measured in two-channel titration injection respirometers (Oroboros, Instruments) [55] at 37°C in a buffer containing 0.5 mM EGTA, 3 mM $MgCl_2$ 60 mM K-lactobionate, 20 mM taurine, 10 mM KH_2PO_4, 20 mM HEPES, 110 mM sucrose and 1 g/l bovine serum albumin. Before each experiment the medium was equilibrated with air in the oxygraph chambers at 37°C until a stable signal was obtained for oxygen calibration. The medium was then replaced by the aerated cell suspensions previously counted and the chambers were closed at a volume of 2 ml by insertion of gas-tight stoppers. The cell suspension was stirred continuously in the respirometer chamber at 460–600 rpm. DatLab software (Oroboros Instruments) was used for data acquisition (1 s time intervals) and analysis, which includes online calculation of the time derivative of oxygen concentration and correction for instrumental background oxygen flux [55]. The respiratory effect of cytochrome *c* was used as a test for plasma membrane integrity and mitochondrial function [55]. After steady-state respiratory flux recording, titration was carried out using oligomycin (1 μg/ml), followed by uncoupling of oxidative phosphorylation by stepwise titration of FCCP up to optimum concentrations in the range of 2.5–4 μM. Finally, respiration was inhibited by sequential addition of 0.5 μM rotenone and 2.5 μM antimycin A. All data were normalized to citrate synthase activity.

Statistical analysis

The results are expressed as means ± SEM. Statistical analysis was performed using a two-tailed *t* test for unpaired variables. Asterisks and crosses in the figure panels refer to statistical probabilities, measured in the various experimental conditions as detailed in the figure legends. Statistical probability values of <0.05 were considered significant.

ACKNOWLEDGEMENTS

We thank Annie Higgs (London) for critically reading the manuscript, Erich Gnaiger (Innsbruck) for his help with respirometry. This work was supported by Telethon Italia (GP007006, to EC), European Community 7^{th} framework programme (OPTISTEM and ENDOSTEM large cooperative programmes, to EC and GC), Cariplo (to EC, MTB and SB), Associazione Italiana Ricerca sul Cancro (AIRC, to EC) Fondazione Romeo ed Enrica Invernizzi (to EC), Association Française contre Les Myopathies (AFM13478, to EC) and Italian Ministry of University (PRIN 2007, to EC). LS is a Senior Telethon Scientist of the Dulbecco-Telethon Institute and an EMBO Young Investigator. SC was a recipient of a fellowship from AIRC.

C.DeP. S.F. and S.P. carried out the majority of experiments and data analysis, and participated in project planning; S.C. and S.P. contributed to the bioenergetics experiments, C.P. prepared the various molecular biology tools, A.D. contributed to time lapse microscopy, R.A. carried out electron microscopy, M.T.B.,G.C., T.P. L.S., carried out some experiments and data analysis and participated in project planning, L.S, S.M. S.B. and E.C. conceived the study, participated in project planning and wrote the paper.

REFERENCES

1. Detmer SA, Chan DC. Functions and dysfunctions of mitochondrial dynamics. *Nat Rev Mol Cell Biol* 2007; **8**(11)**:** 870-9.

2. Dimmer KS, Scorrano L. (De)constructing mitochondria: what for? *Physiology (Bethesda)* 2006; **21:** 233-41.

3. Santel A, Frank S. Shaping mitochondria: The complex posttranslational regulation of the mitochondrial fission protein DRP1. *IUBMB Life* 2008; **60**(7)**:** 448-55.

4. Skulachev VP. Mitochondrial filaments and clusters as intracellular power-transmitting cables. *Trends Biochem Sci* 2001; **26**(1)**:** 23-9.

5. Westermann B. Molecular machinery of mitochondrial fusion and fission. *J Biol Chem* 2008; **283**(20)**:** 13501-5.

6. Campello S, Lacalle RA, Bettella M, Manes S, Scorrano L, Viola A. Orchestration of lymphocyte chemotaxis by mitochondrial dynamics. *J Exp Med* 2006; **203**(13)**:** 2879-86.

7. Chen H, Detmer SA, Ewald AJ, Griffin EE, Fraser SE, Chan DC. Mitofusins Mfn1 and Mfn2 coordinately regulate mitochondrial fusion and are essential for embryonic development. *J Cell Biol* 2003; **160**(2)**:** 189-200.

8. Finkel T, Hwang PM. The Krebs cycle meets the cell cycle: mitochondria and the G1-S transition. *Proc Natl Acad Sci U S A* 2009; **106**(29)**:** 11825-6.

9. Puigserver P, Spiegelman BM. Peroxisome proliferator-activated receptor-gamma coactivator 1 alpha (PGC-1 alpha): transcriptional coactivator and metabolic regulator. *Endocr Rev* 2003; **24**(1)**:** 78-90.

10. Wenz T, Diaz F, Spiegelman BM, Moraes CT. Activation of the PPAR/PGC-1alpha pathway prevents a bioenergetic deficit and effectively improves a mitochondrial myopathy phenotype. *Cell Metab* 2008; **8**(3)**:** 249-56.

11. Hood DA, Irrcher I, Ljubicic V, Joseph AM. Coordination of metabolic plasticity in skeletal muscle. *J Exp Biol* 2006; **209**(Pt 12)**:** 2265-75.

12. Bach D, Pich S, Soriano FX, Vega N, Baumgartner B, Oriola J *et al.* Mitofusin-2 determines mitochondrial network architecture and mitochondrial metabolism. A novel regulatory mechanism altered in obesity. *J Biol Chem* 2003; **278**(19)**:** 17190-7.

13. Sciorati C, Galvez BG, Brunelli S, Tagliafico E, Ferrari S, Cossu G *et al.* Ex vivo treatment with nitric oxide increases mesoangioblast therapeutic efficacy in muscular dystrophy. *J Cell Sci* 2006; **119**(Pt 24)**:** 5114-23.

14. Garthwaite J, Southam E, Boulton CL, Nielsen EB, Schmidt K, Mayer B. Potent and selective inhibition of nitric oxide-sensitive guanylyl cyclase by 1H-[1,2,4]oxadiazolo[4,3-a]quinoxalin-1-one. *Mol Pharmacol* 1995; **48**(2)**:** 184-8.

15. Stamler JS, Meissner G. Physiology of nitric oxide in skeletal muscle. *Physiol Rev* 2001; **81**(1)**:** 209-237.

16. van der Bliek AM, Redelmeier TE, Damke H, Tisdale EJ, Meyerowitz EM, Schmid SL. Mutations in human dynamin block an intermediate stage in coated vesicle formation. *J Cell Biol* 1993; **122**(3)**:** 553-63.

17. Angelin A, Tiepolo T, Sabatelli P, Grumati P, Bergamin N, Golfieri C *et al.* Mitochondrial dysfunction in the pathogenesis of Ullrich congenital muscular dystrophy and prospective therapy with cyclosporins. *Proc Natl Acad Sci U S A* 2007; **104**(3)**:** 991-6.

18. Moncada S, Palmer RM, Higgs EA. Nitric oxide: physiology, pathophysiology, and pharmacology. *Pharmacol Rev* 1991; **43**(2)**:** 109-42.

19. Carlucci A, Lignitto L, Feliciello A. Control of mitochondria dynamics and oxidative metabolism by cAMP, AKAPs and the proteasome. *Trends Cell Biol* 2008; **18**(12)**:** 604-13.

20. Cereghetti GM, Stangherlin A, Martins de Brito O, Chang CR, Blackstone C, Bernardi P *et al.* Dephosphorylation by calcineurin regulates translocation of Drp1 to mitochondria. *Proc Natl Acad Sci U S A* 2008; **105**(41)**:** 15803-8.

21. Barsoum MJ, Yuan H, Gerencser AA, Liot G, Kushnareva Y, Graber S *et al.* Nitric oxide-induced mitochondrial fission is regulated by dynamin-related GTPases in neurons. *Embo J* 2006; **25**(16)**:** 3900-11.

22. Cho DH, Nakamura T, Fang J, Cieplak P, Godzik A, Gu Z *et al.* S-nitrosylation of Drp1 mediates beta-amyloid-related mitochondrial fission and neuronal injury. *Science* 2009; **324**(5923)**:** 102-5.23.

23- Acin-Perez R, Salazar E, Kamenetsky M, Buck J, Levin LR, Manfredi G. Cyclic AMP produced inside mitochondria regulates oxidative phosphorylation. *Cell Metab* 2009; **9**(3)**:** 265-76.

24. Thippeswamy T, McKay JS, Quinn JP, Morris R. Nitric oxide, a biological double-faced janus--is this good or bad? *Histol Histopathol* 2006; **21**(4)**:** 445-58.

25. Moncada S, Bolanos JP. Nitric oxide, cell bioenergetics and neurodegeneration. *J Neurochem* 2006; **97**(6)**:** 1676-89.

26. Wakabayashi J, Zhang Z, Wakabayashi N, Tamura Y, Fukaya M, Kensler TW *et al.* The dynamin-related GTPase Drp1 is required for embryonic and brain development in mice. *J Cell Biol* 2009; **186**(6)**:** 805-16.

27. Brenman JE, Chao DS, Xia H, Aldape K, Bredt DS. Nitric oxide synthase complexed with dystrophin and absent from skeletal muscle sarcolemma in Duchenne muscular dystrophy. *Cell* 1995; **82**(5)**:** 743-52.

28. Erusalimsky JD, Moncada S. Nitric oxide and mitochondrial signaling: from physiology to pathophysiology. *Arterioscler Thromb Vasc Biol* 2007; **27**(12)**:** 2524-31.

29. Brunelli S, Rovere-Querini P, Sciorati C, Manfredi AA, Clementi E. Nitric oxide: emerging concepts about its use in cell-based therapies. *Expert Opin Investig Drugs* 2007; **16**(1)**:** 33-43.

30. Herrmann PC, Herrmann EC. Oxygen metabolism and a potential role for cytochrome c oxidase in the Warburg effect. *J Bioenerg Biomembr* 2007; **39**(3)**:** 247-50.

31. Colussi C, Mozzetta C, Gurtner A, Illi B, Rosati J, Straino S *et al.* HDAC2 blockade by nitric oxide and histone deacetylase inhibitors reveals a common target in Duchenne muscular dystrophy treatment. *Proc Natl Acad Sci U S A* 2008.

32. Pisconti A, Brunelli S, Di Padova M, De Palma C, Deponti D, Baesso S *et al.* Follistatin induction by nitric oxide through cyclic GMP: a tightly regulated signaling pathway that controls myoblast fusion. *J Cell Biol* 2006; **172**(2)**:** 233-44.

33. Ouchi N, Oshima Y, Ohashi K, Higuchi A, Ikegami C, Izumiya Y *et al.* Follistatin-like 1, a Secreted Muscle Protein, Promotes Endothelial Cell Function and Revascularization in Ischemic Tissue through a Nitric-oxide Synthase-dependent Mechanism. *J Biol Chem* 2008; **283**(47)**:** 32802-11.

34. Kaliman P, Canicio J, Testar X, Palacin M, Zorzano A. Insulin-like growth factor-II, phosphatidylinositol 3-kinase, nuclear factor-kappaB and inducible nitric-oxide synthase define a common myogenic signaling pathway. *J Biol Chem* 1999; **274**(25)**:** 17437-44.

35. Brunelli S, Sciorati C, D'Antona G, Innocenzi A, Covarello D, Galvez BG *et al.* Nitric oxide release combined with nonsteroidal antiinflammatory activity prevents muscular dystrophy pathology and enhances stem cell therapy. *Proc Natl Acad Sci U S A* 2007; **104**(1)**:** 264-9.

36. Anderson JE. A role for nitric oxide in muscle repair: nitric oxide-mediated activation of muscle satellite cells. *Mol Biol Cell* 2000; **11**(5)**:** 1859-74.

37. Moncada S, Erusalimsky JD. Does nitric oxide modulate mitochondrial energy generation and apoptosis? *Nat Rev Mol Cell Biol* 2002; **3**(3)**:** 214-20.

38. Clementi E, Brown GC, Foxwell N, Moncada S. On the mechanism by which vascular endothelial cells regulate their oxygen consumption. *Proc Natl Acad Sci U S A* 1999; **96**(4)**:** 1559-62.

39. Nisoli E, Clementi E, Paolucci C, Cozzi V, Tonello C, Sciorati C *et al.* Mitochondrial biogenesis in mammals: the role of endogenous nitric oxide. *Science* 2003; **299**(5608)**:** 896-9.

40. Nisoli E, Falcone S, Tonello C, Cozzi V, Palomba L, Fiorani M *et al.* Mitochondrial biogenesis by NO yields functionally active mitochondria in mammals. *Proc Natl Acad Sci U S A* 2004; **101**(47)**:** 16507-12.

41. Lin J, Wu H, Tarr PT, Zhang CY, Wu Z, Boss O *et al.* Transcriptional co-activator PGC-1 alpha drives the formation of slow-twitch muscle fibres. *Nature* 2002; **418**(6899)**:** 797-801.

42. Figueiredo PA, Mota MP, Appell HJ, Duarte JA. The role of mitochondria in aging of skeletal muscle. *Biogerontology* 2008; **9**(2)**:** 67-84.

43. Wehling M, Spencer MJ, Tidball JG. A nitric oxide synthase transgene ameliorates muscular dystrophy in mdx mice. *J Cell Biol* 2001; **155**(1)**:** 123-31.

44. Wells GD, Noseworthy MD, Hamilton J, Tarnopolski M, Tein I. Skeletal muscle metabolic dysfunction in obesity and metabolic syndrome. *Can J Neurol Sci* 2008; **35**(1)**:** 31-40.

45. Cossu G, Eusebi F, Grassi F, Wanke E. Acetylcholine receptor channels are present in undifferentiated satellite cells but not in embryonic myoblasts in culture. *Dev Biol* 1987; **123**(1)**:** 43-50.

46. Bulotta S, Barsacchi R, Rotiroti D, Borgese N, Clementi E. Activation of the endothelial nitric-oxide synthase by tumor necrosis factor-alpha. A novel feedback mechanism regulating cell death. *J Biol Chem* 2001; **276**(9)**:** 6529-36.

47. Cipolat S, Martins de Brito O, Dal Zilio B, Scorrano L. OPA1 requires mitofusin 1 to promote mitochondrial fusion. *Proc Natl Acad Sci U S A* 2004; **101**(45)**:** 15927-32.

48. Abramoff MD, Viergever MA. Computation and visualization of three-dimensional soft tissue motion in the orbit. *IEEE Trans Med Imaging* 2002; **21**(4)**:** 296-304.

49. Collins TJ, Berridge MJ, Lipp P, Bootman MD. Mitochondria are morphologically and functionally heterogeneous within cells. *Embo J* 2002; **21**(7)**:** 1616-27.

50. Varadi A, Johnson-Cadwell LI, Cirulli V, Yoon Y, Allan VJ, Rutter GA. Cytoplasmic dynein regulates the subcellular distribution of mitochondria by controlling the recruitment of the fission factor dynamin-related protein-1. *J Cell Sci* 2004; **117**(Pt 19)**:** 4389-400.

51. Ishihara N, Eura Y, Mihara K. Mitofusin 1 and 2 play distinct roles in mitochondrial fusion reactions via GTPase activity. *J Cell Sci* 2004; **117**(Pt 26)**:** 6535-46.

52. Brini M, De Giorgi F, Murgia M, Marsault R, Massimino ML, Cantini M *et al.* Subcellular analysis of Ca2+ homeostasis in primary cultures of skeletal muscle myotubes. *Mol Biol Cell* 1997; **8**(1)**:** 129-43.

53. Manfredi G, Yang L, Gajewski CD, Mattiazzi M. Measurements of ATP in mammalian cells. *Methods* 2002; **26**(4)**:** 317-26.

54. Robinson BH. Use of fibroblast and lymphoblast cultures for detection of respiratory chain defects. *Methods Enzymol* 1996; **264:** 454-64.

55. Gnaiger E. Bioenergetics at low oxygen: dependence of respiration and phosphorylation on oxygen and adenosine diphosphate supply. *Respir Physiol* 2001; **128**(3)**:** 277-97.

FIGURE LEGENDS

Figure 1 NO regulates myogenesis and mitochondrial network formation via cGMP.

Myogenic precursor cells transfected with the red fluorescent mitochondrial protein mitoDsRed were treated with L-NAME, ODQ or vehicle (C) and differentiated by serum withdrawal for up to 12 h.

(**a**) Mitochondrial morphology detected by transient transfection with mitoDsRed; nuclei are stained for MyoD (blue) to distinguish myogenic cells from possible contaminating cells. Bar: 10 μm.

(**b**) Expression of the differentiation markers Mef 2A, Myo D, myogenin and sarcomeric myosin (MyHC) detected by western blot analysis.

(**c**) Expression of the mitochondrial proteins mitofusins (Mfn) 1 and 2, Opa1, Drp1, cytochrome *c* (CytC) and cytochrome *c* oxidase subunit 4 (COX IV). Calnexin was used as a loading control in both B and C.

(**d**) NOS activity measured as the conversion of ^{3}H L-arginine into ^{3}H L-citrulline. The inset shows the levels of expression of nNOS during myogenic differentiation. Calnexin (Clx) was used as a loading control.

(**e**) Generation of cyclic GMP. Images are from one of four independent reproducible experiments; graphs represent the values ± SEM (n = 4).

Figure 2 Inhibition of myogenesis and mitochondrial network formation by NO removal are not due to toxic effects.

Myogenic precursor cells were treated with L-NAME, ODQ or vehicle (C) and differentiated by serum withdrawal for up to 72 h, during which time the rate of spontaneous apoptosis was measured.

(**a**) Phosphatidylserine exposure to the plasma membrane in 7-amino actinomycin D-excluding cells.

(**b**) Number of trypan blue-excluding cells.

(**c**) Expression of procaspase9 and its cleaved form, and of cleaved caspase 3. Images are from one of three independent reproducible experiments; graphs represent the values ± SEM (n = 3).

Figure 3 NO and cGMP regulate mitochondrial dynamics.

(**a**) Myogenic precursor cells were co-transfected with vectors coding for mitoDsRed and cytosolic YFP (pEN1YFP) and differentiated. L-NAME, ODQ or vehicle (C) were added after 6 h of differentiation and mitochondrial morphology examined by time-lapse microscopy at the indicated time-points. Images are representative of three independent reproducible experiments. Bar: 10 μm.

(**b**, **c**) Myogenic precursor cells were transfected with the mitoDsRed coding vector and differentiated. Six h later cells were treated with L-NAME, ODQ, DETA-NO, 8Br-cGMP or vehicle (C) in various combinations as indicated, fixed and examined after 50 min. Red and blue in **b** show the staining of mitoDsRed and an anti MyoD Ab, respectively. Bar: 10 μm.

(**c**) Fifteen random fields per sample were acquired and the fragmentation index was established using the imagetool 3.0 software. Dimension ranges for fragmented and elongated were 1.20 μm ± 0.2 and > 3.50 μm, respectively. Asterisks show statistical probability vs. C, crosses vs. L-NAME and circles vs. ODQ ($P < 0.001$).

Figure 4 NO and cGMP stimulate myogenesis through inhibition of mitochondrial fission.

(**a,b**) Myogenic precursor cells were transfected with the vector coding for either mitoGFP (green) or mitoDsRed (red), mixed, differentiated for 6 h, and exposed for 1 h to L-NAME, ODQ, DETA-NO, 8Br-cGMP or vehicle (C) as indicated. Plasma membrane fusion was induced by addition of polyethylene glycol 1500 and mitochondrial fusion events quantified after 2, 4 and 6 h in the heteropolykaryons by measuring the fraction of mitochondria simultaneously positive for both mtGFP and mitoDsRed (colocalization index %; $n = 3$). Bar: 10 μM.

(**c**) Myogenic precursor cells were transfected with vectors coding for the cytosolic marker pEYFP-N1 (green) or the dominant negative Drp1, pEYFP-N1-DRPK38A, and differentiated in the presence of L-NAME and ODQ. Mitochondrial morphology was assessed after 6 h. Bar: 10 μM.

(**d**) Expression of the myogenic differentiation markers Mef 2A, MyoD, myogenin and sarcomeric myosin (MyHC) was determined by western blotting in myogenic precursors transfected with either the empty pCDNA3 vector or the dominant negative Drp1 (pcDNA3-Drp1 K38A) at the indicated time-points. The result of one out of three reproducible experiments is shown.

Figure 5 NO and cGMP control activity and localization of Drp1.

Myogenic precursor cells were differentiated for 6 h and treated for 1 h with L-NAME, ODQ, DETA-NO, 8Br-cGMP or vehicle (C), added as indicated.

(**a**) Cells were fractionated and mitochondrial (MT), microsomal (MI) and cytosolic (CI) fractions examined for Drp1 content by western blotting, using GAPDH and COX IV as loading controls for cytosolic and mitochondrial proteins, respectively. Results shown in the images are representative of five reproducible experiments, which are quantified in the corresponding graphs.

(**b**) co-immunoprecipitation of Drp1 with Fis1 was carried out using the anti Fis1 Ab for immunoprecipitation (IP). The amount of co-immunoprecipitated Drp1 was revealed by immuno blotting (IB) using a specific anti Drp1 Ab. As control the amount of Fis1 immunoprecipitated was also checked by IB. As a further control of specificity we checked the absence of coimmunoprecipitation of Drp 1 with calnexin.

(**c**) Drp1 GTPase activity was measured in pull down experiments using GTP-conjugated beads. The representative images shown in B and C are from four independent reproducible experiments. The graphs below each image report the densitometric values ± SEM of the relevant band from the four experiments. In all panels, asterisks, crosses and circles show statistical probability ($P < 0.001$), calculated vs. C, L-NAME and ODQ, respectively.

Figure 6 NO/cGMP triggers G kinase-dependent phosphorylation of Drp1

(**a**) Myc-Drp1 was immunoprecipitated from [^{32}P]orthophosphate-labelled proliferating or differentiating myogenic precursor cells. Immunoprecipitates were resolved by SDS-PAGE and ^{32}P-labelled-Myc-Drp1 was visualized by autoradiography

(**b**) Myc-Drp1 was immunoprecipitated from [^{32}P]orthophosphate-labelled myogenic precursor cells treated with DETA-NO, 8Br cGMP with or without KT5823 and ODQ, respectively, or BAY41-2272. Immunoprecipitates were resolved by SDS-PAGE and ^{32}P-labelled-Myc-Drp1 was visualized by autoradiography

Figure 7 Bioenergetic consequences of regulation of fission by NO and cGMP.

Myogenic precursor cells were transfected with pEYFP-N1 or pEYFP-N1-Drp1 K38A, differentiated (diff) or allowed to proliferate (pro) for 6 h and treated as specified.

(**a**) Cells were loaded with the mitochondrial potentiometric dye TMRM and mitochondrial membrane potential was measured 1 h after treatment with vehicle (C) or ODQ. Arrows mark the addition of oligomycin (O; 1 μg/ml) and FCCP (4 μM).

(**b,c**) Cells were loaded with luciferin-luciferase and ATP generated through oxidative phosphorylation (**b**) or glycolysis (**c**) was measured after addition of vehicle or ODQ.

(**d**,**e**) Respiratory function was measured in a high sensitivity respirometer. The values are shown for total, oligomycin-resistant, maximal (uncoupled) and residual oxygen consumption (ROC), as well as the ratio of oligomycin-resistant to maximal (oligomycin resistant/M) and coupled (total minus oligomycin resistant) to maximal (C/M).

(**f**) Activity of the mitochondrial respiratory complexes measured as in A assessing ATP generation in cells respiring on pyruvate-malate (P+M) or glutamate-malate (G+M) (complex I), succinate-rotenone (S+Rot) (complex II), TMPD-ascorbate-antimycin A (T+A+AntA) (complex IV). The panels show values ± SEM (n = 4). Double ($P < 0.01$) and triple ($P < 0.001$) asterisks and crosses show statistical probability vs. control and ODQ, respectively.

Figure 8 NO/cGMP protect from H_2O_2-induced apoptosis via inhibition of Drp1

Myogenic precursor cells were transfected with pcDNA3-Drp1-myc or pcDNA3-Drp1 K38A-myc and differentiated for 6 h. Cells were then exposed to H_2O_2 or vehicle in the presence or absence of L-NAME or ODQ.

(**a**) Phosphatidylserine exposure to the plasma membrane in 7-amino actinomycin D-excluding cells.

(**b**) Number of trypan blue-excluding cells.

The panels show values ± SEM (n = 4). Asterisks and crosses show significant differences ($P < 0.001$) from C of L-NAME or ODQ-treated cells expressing pcDNA-myc, and of pCDNA3-Drp1 K38A-expressing cells from the cells expressing the empty vector, respectively.

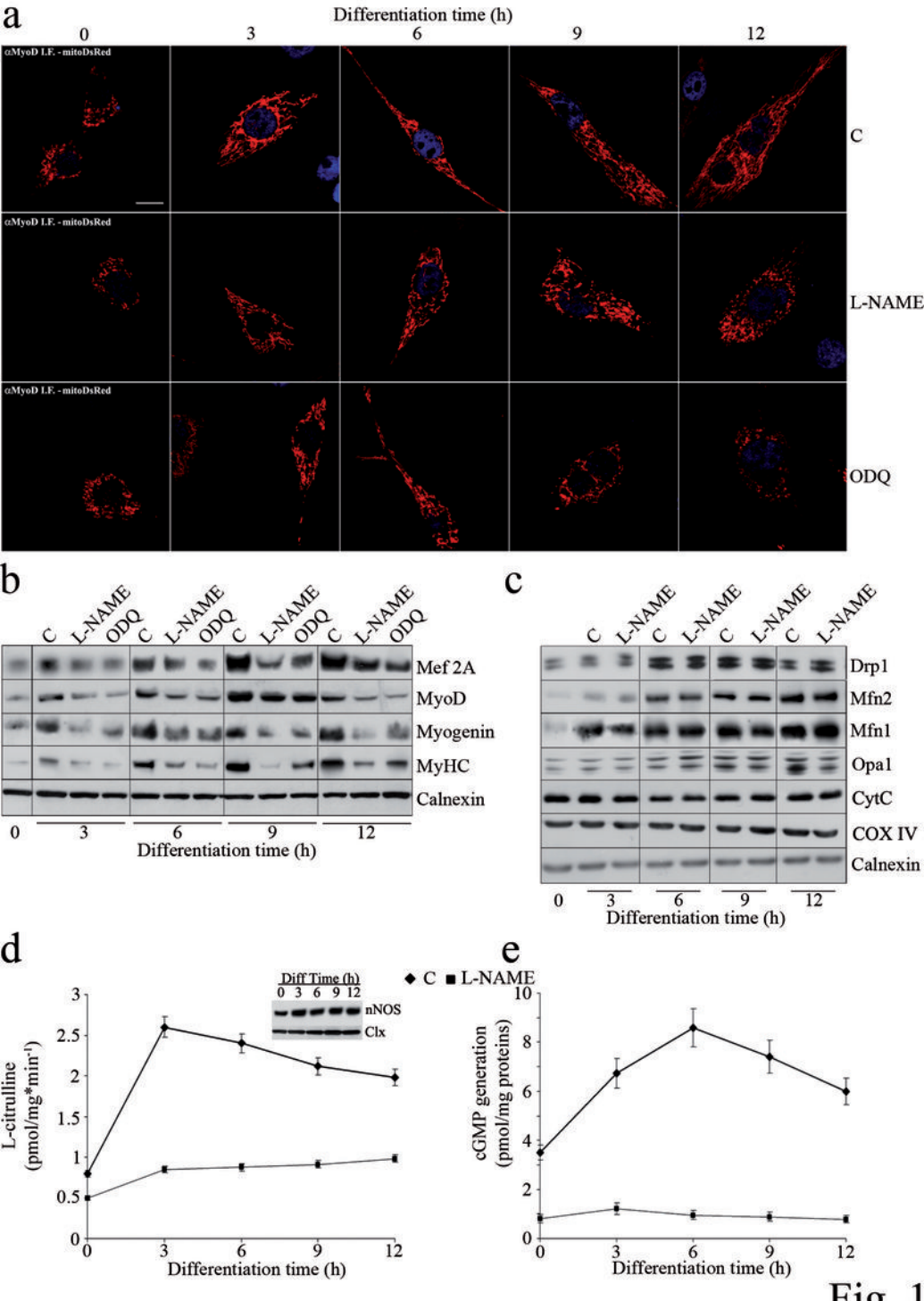
a
Differentiation time (h)
0
3
6
9
12
αMyoD I.F. - mitoDsRed
C
L-NAME
ODQ
b
C
L-NAME
ODQ
Mef 2A
MyoD
Myogenin
MyHC
Calnexin
Differentiation time (h)
c
Drp1
Mfn2
Mfn1
Opa1
CytC
COX IV
Calnexin
d
Diff Time (h)
C
L-NAME
nNOS
Clx
L-citrulline (pmol/mg*min-1)
e
cGMP generation (pmol/mg proteins)

Fig. 1

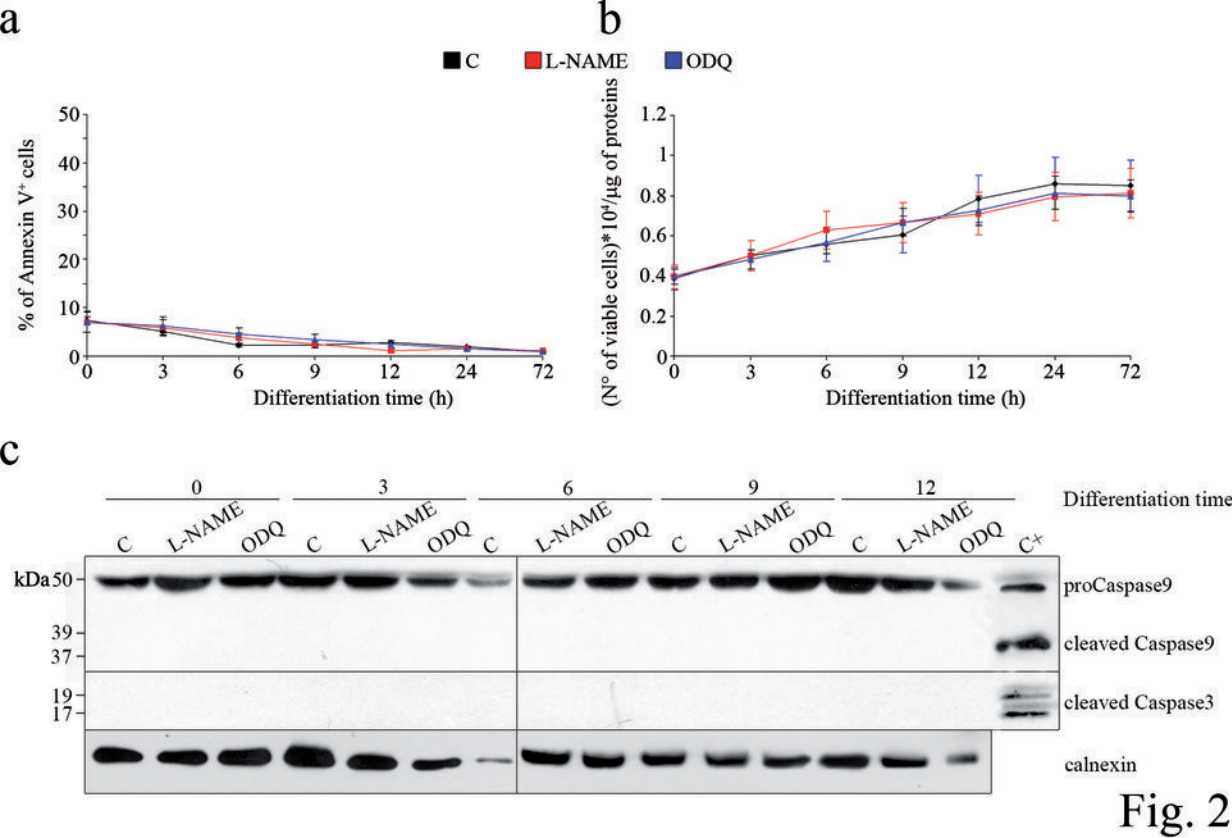
a
b
C
L-NAME
ODQ
% of Annexin V+ cells
(N° of viable cells)*10⁴/µg of proteins
Differentiation time (h)
Differentiation time (h)
c
Differentiation time
0
3
6
9
12
C
L-NAME
ODQ
C+
kDa
50
39
37
19
17
proCaspase9
cleaved Caspase9
cleaved Caspase3
calnexin

Fig. 2

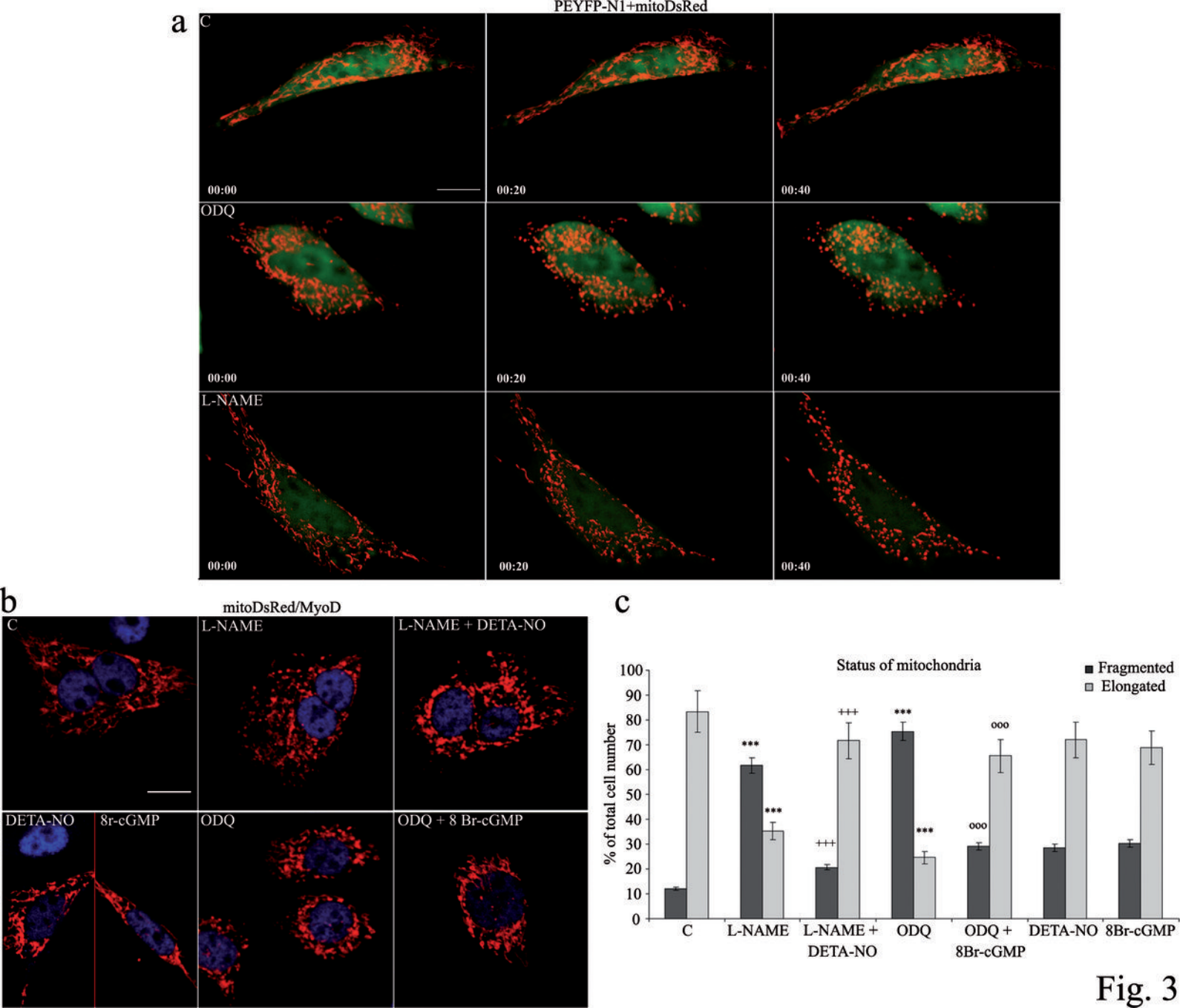
a
PEYFP-N1+mitoDsRed
C
00:00
00:20
00:40
ODQ
00:00
00:20
00:40
L-NAME
00:00
00:20
00:40
b
mitoDsRed/MyoD
C
L-NAME
L-NAME + DETA-NO
DETA-NO
8r-cGMP
ODQ
ODQ + 8 Br-cGMP
c
Status of mitochondria
Fragmented
Elongated
% of total cell number
100
90
80
70
60
50
40
30
20
10
0
***
+++
ooo
C
L-NAME
L-NAME + DETA-NO
ODQ
ODQ + 8Br-cGMP
DETA-NO
8Br-cGMP

Fig. 3

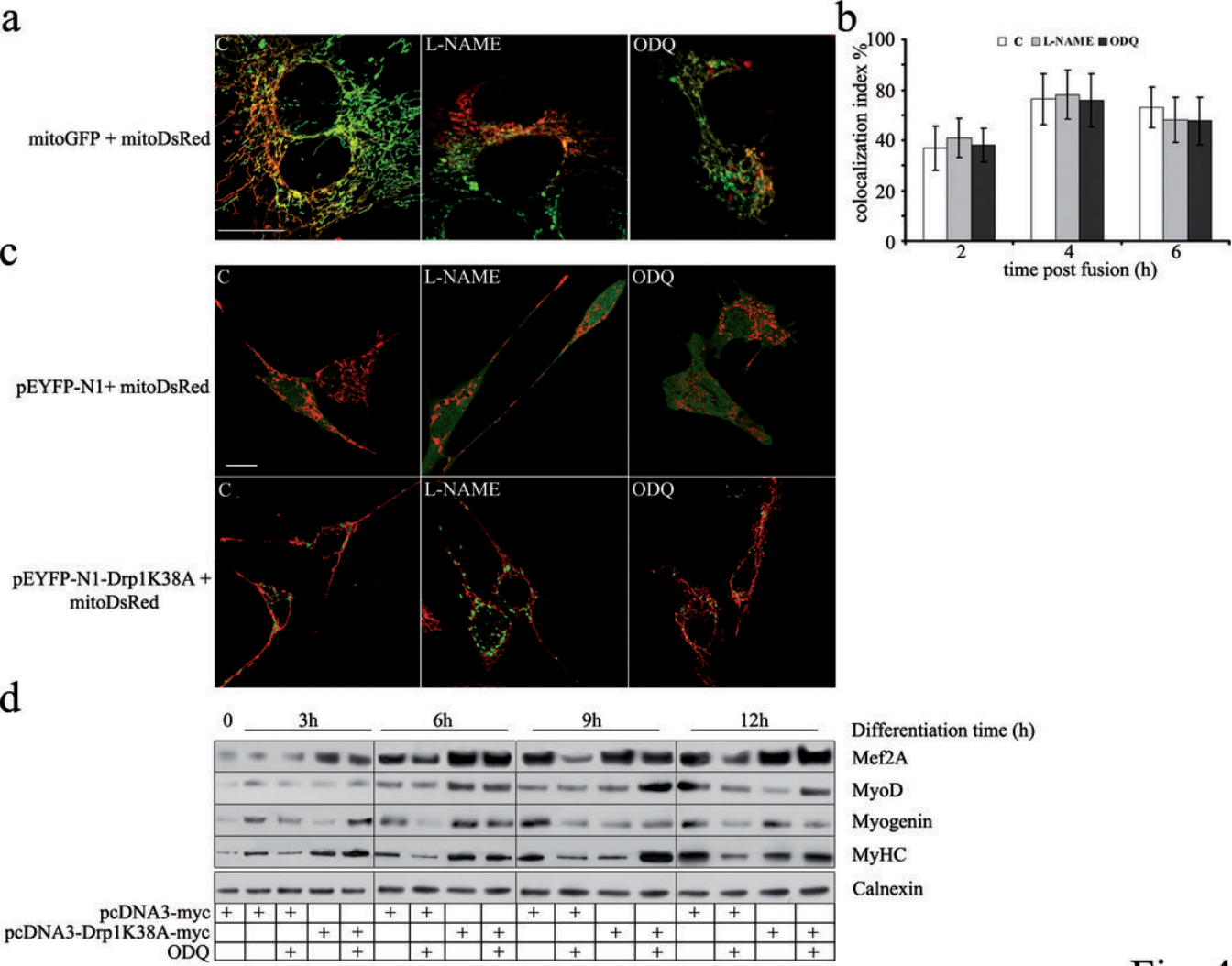
a
C
L-NAME
ODQ
mitoGFP + mitoDsRed
b
C
L-NAME
ODQ
colocalization index %
100
80
60
40
20
0
2
4
6
time post fusion (h)
c
C
L-NAME
ODQ
pEYFP-N1+ mitoDsRed
C
L-NAME
ODQ
pEYFP-N1-Drp1K38A + mitoDsRed
d
0
3h
6h
9h
12h
Differentiation time (h)
Mef2A
MyoD
Myogenin
MyHC
Calnexin
pcDNA3-myc
pcDNA3-Drp1K38A-myc
ODQ

Fig. 4

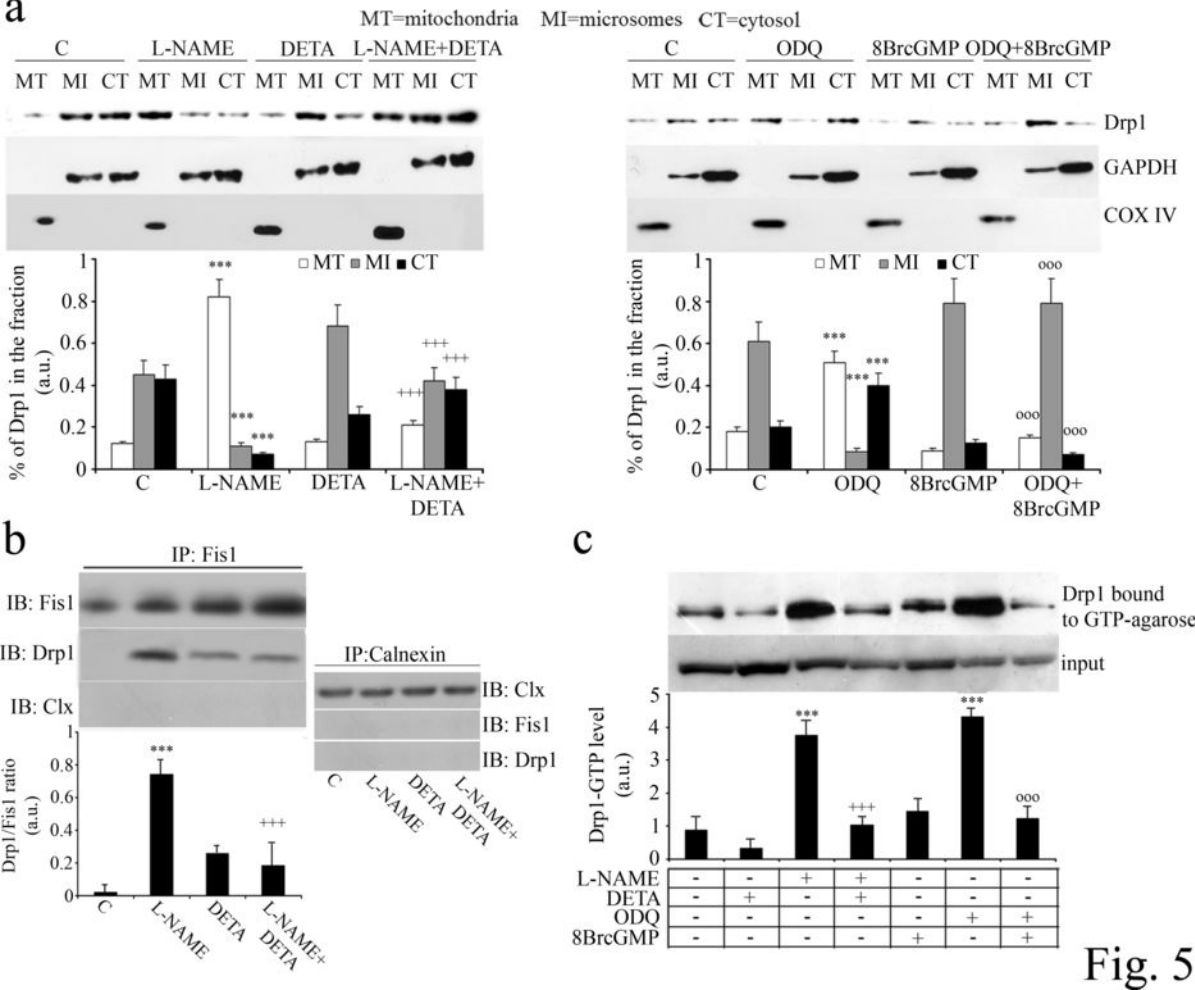
a
MT=mitochondria MI=microsomes CT=cytosol
C
L-NAME
DETA
L-NAME+DETA
MT MI CT MT MI CT MT MI CT MT MI CT
Drp1
GAPDH
COX IV
% of Drp1 in the fraction (a.u.)
MT MI CT
C
L-NAME
DETA
L-NAME+ DETA
ODQ
8BrcGMP
ODQ+8BrcGMP
ODQ+ 8BrcGMP
b
IP: Fis1
IB: Fis1
IB: Drp1
IB: Clx
IP:Calnexin
Drp1/Fis1 ratio (a.u.)
c
Drp1 bound to GTP-agarose
input
Drp1-GTP level (a.u.)
L-NAME
DETA
ODQ
8BrcGMP

Fig. 5

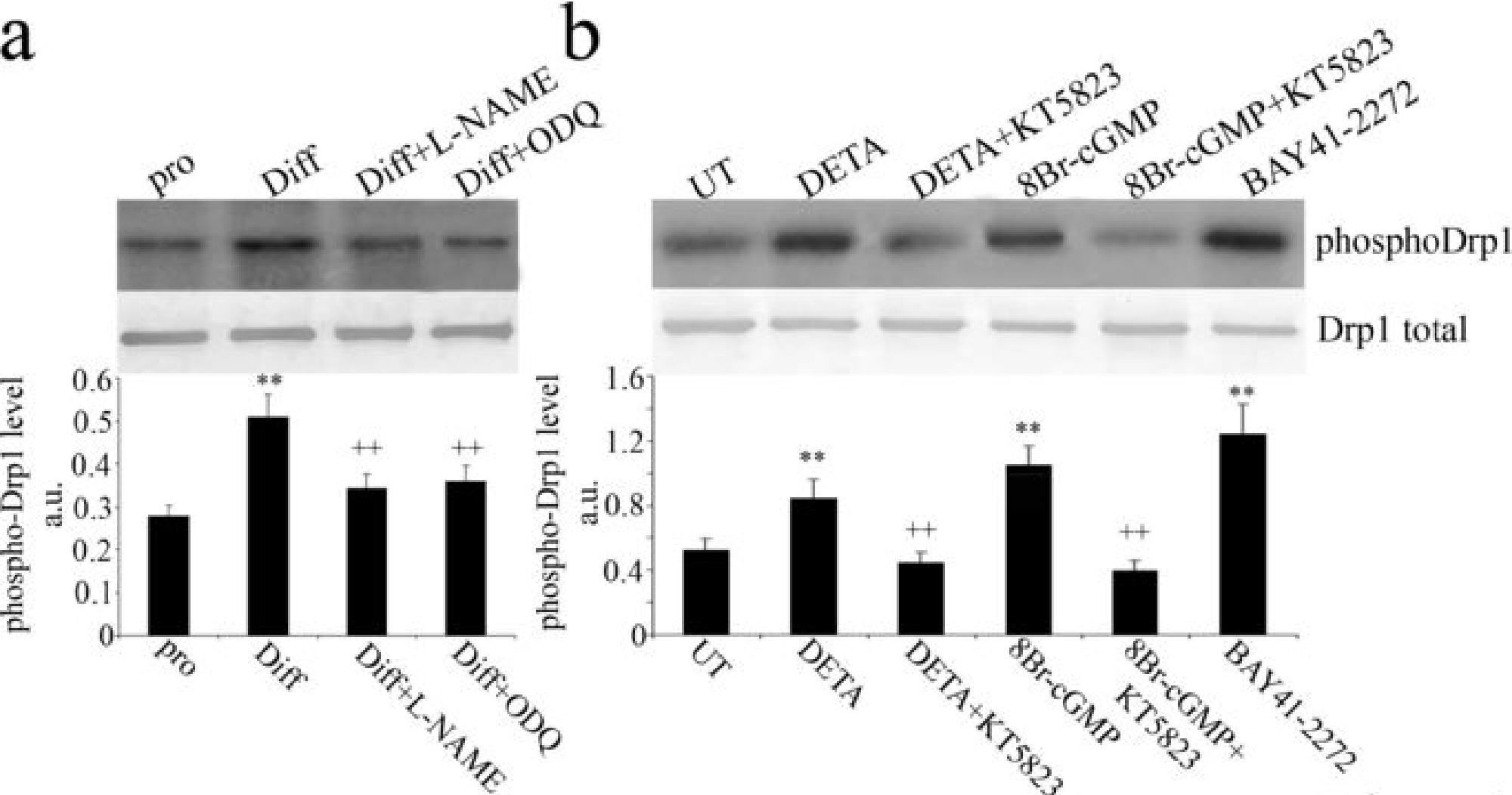
a
b
pro
Diff
Diff+L-NAME
Diff+ODQ
UT
DETA
DETA+KT5823
8Br-cGMP
8Br-cGMP+KT5823
BAY41-2272
phosphoDrp1
Drp1 total
phospho-Drp1 level
a.u.
0.6
0.5
0.4
0.3
0.2
0.1
0
1.6
1.2
0.8
0.4
**
++
8Br-cGMP+ KT5823

Fig. 6

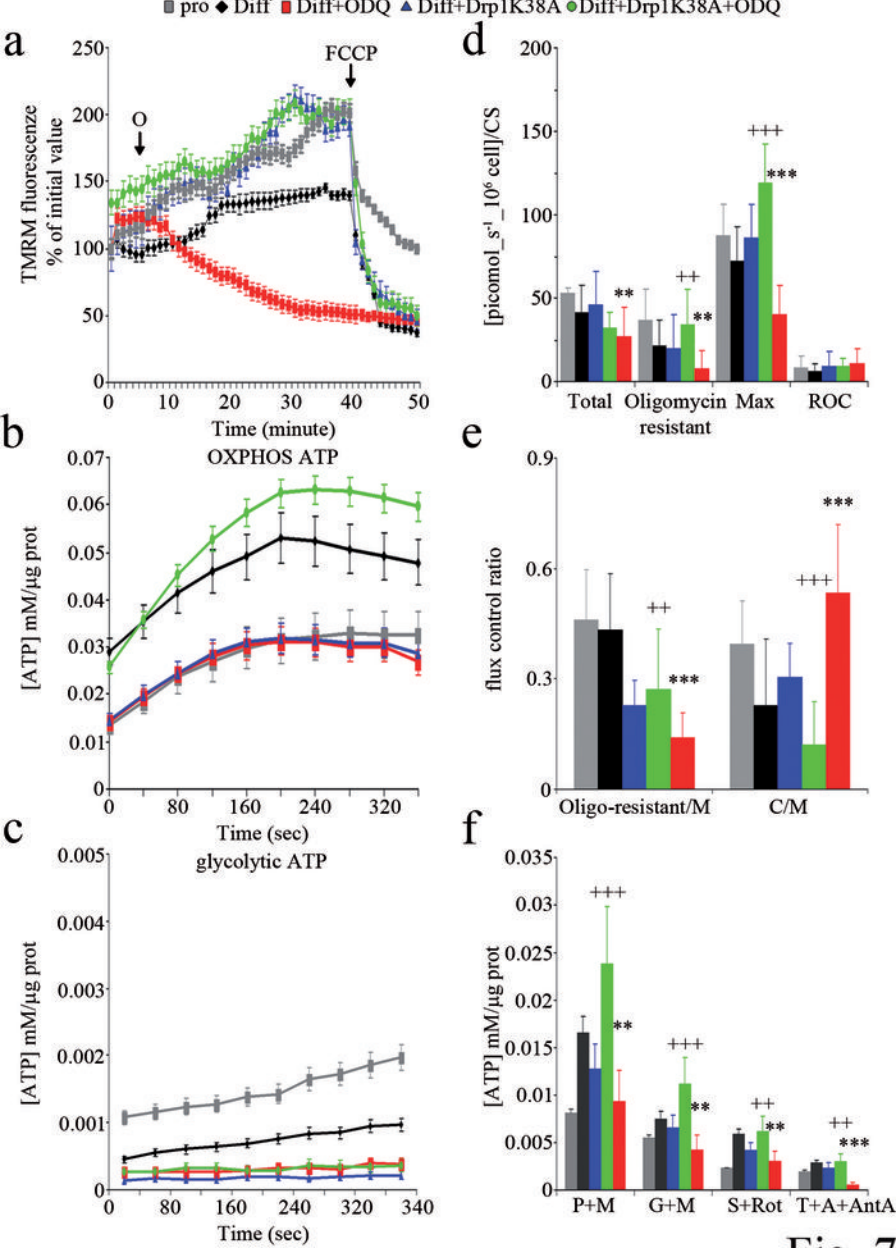
pro ◆ Diff ■ Diff+ODQ ▲ Diff+Drp1K38A ● Diff+Drp1K38A+ODQ
a
FCCP
O
TMRM fluorescenze
% of initial value
Time (minute)
b
OXPHOS ATP
[ATP] mM/µg prot
Time (sec)
c
glycolytic ATP
[ATP] mM/µg prot
Time (sec)
d
[picomol_s⁻¹_10⁶ cell]/CS
Total
Oligomycin resistant
Max
ROC
e
flux control ratio
Oligo-resistant/M
C/M
f
[ATP] mM/µg prot
P+M
G+M
S+Rot
T+A+AntA

Fig. 7

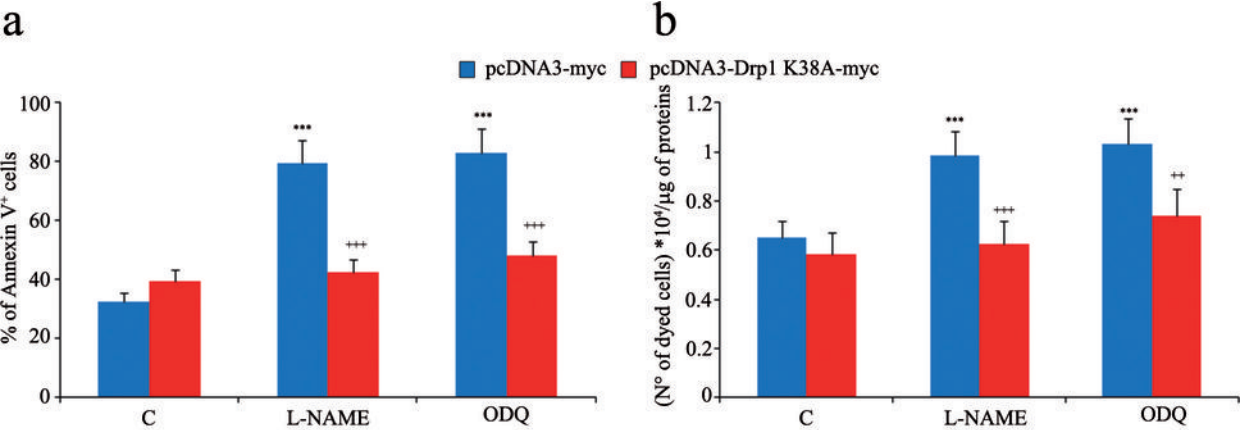
a
b
pcDNA3-myc
pcDNA3-Drp1 K38A-myc
% of Annexin V+ cells
(N° of dyed cells) *10⁴/µg of proteins
C
L-NAME
ODQ
***
+++
++

Fig. 8